 SL, vol.8, no.2, pp.71-81, 2012

Control Effect of Fatigue Crack Propagation in the TiNi Fiber Reinforced Smart Composite

A. Shimamoto[1], C. C. Lee[2], Y. Furuya[3]

Abstract: The TiNi fiber reinforced / PC composite material was developed, and shape memory effect, which would prevent fatigue crack growth, of the material was investigated through fatigue experiments. The fatigue behavior and crack propagation were observed under various temperature in the SEM servopulser, which is a fatigue testing instrument with scanning electron microscope. The results showed the effectiveness of fatigue resistance. The shape memory effect and expansion behavior of the matrix caused by increasing temperature created the fatigue crack propagation control mechanism. It was verified that the controlling of fatigue crack growth was attributed to the compressive stress field in the matrix which was caused by shrinkage of the TiNi fiber above austenitic finishing temperature (A_f).

Keywords: Shape Memory Alloy, Polycarbonate Composite, Fatigue, Crack Closure, Crack Propagation, Shrinkage Effect.

1 Introduction

A shape memory alloy fiber reinforced composite had been developed as a new type of smart composites. Shape memory TiNi fiber was used for reinforcing and actuating the mechanical properties of composites (Rogers 1991, Furuya 1993). The unique property, which a SMA composite inherited at and above the inverse phase transformation temperature of TiNi alloy, could be utilized to strengthen and control crack fatigue propagation in a composite. The compressive stress resulted from the shape memory effect during martensite to austenite phase transformation in SMA could reduce stress concentration at a crack tip and suppress fatigue crack propagation. The authors had experimentally confirmed large compressive stress in a matrix and following suppression effect in the vicinity of a crack-tip. Embedded fiber in the shape memory TiNi fiber reinforced epoxy composite as well as

[1] Saitama Institute of Technology, JAPAN
[2] Sumita Optical Glass Inc., JAPAN
[3] Department of Intelligent Machines and System Engineering, Hirosaki University, JAPAN

the aluminum matrix composite reduced stress concentration (Shimamoto, 1991, 1995, 1997, 1999, 2002, 2003). Such studies contributed to make SMA composites into practical applications. There had been a few studies related to the fatigue of SMA composites. Quantitative and systematic researches on fatigue crack propagation behaviors and the crack closure mechanisms of SMA composites were still open yet. In this paper, the photo-elastic method and the fine-grid method were employed to verify the characteristics of the intelligent composite material which utilized the mechanical properties of SMA. The fine-grid method was originally developed by the authors for local strain measurement. It allowed observing crack-tip deformation and following propagation behavior near embedded fiber (Shimamoto, 1991, 2004). The fatigue crack propagation and the crack-closure behavior were analyzed by the hysteresis curve, which described crack-tip displacement under applied load. Fatigue crack retardation, crack-tip deformation and crack closure behavior were discussed with the elastic stress distribution in the domain around embedded inhomogeneous fiber in a composite.

2 Experimental

2.1 Specimen

The TiNi fiber reinforced polycarbonate composites were developed by the authors. The shape memorized TiNi fiber was embedded in the polycarbonate matrix. TiNi fiber's volume ratio to the polycarbonate matrix was 0.8%. The mechanical properties of the specimens were summarized on Table 1.

Table 1: Mechanical properties of constituents

Material	Polycarbonate		TiNi fiber	
Temperature	20^oC	80^oC	20^oC	80^oC
Young's Modulus	2.1GPa	1.9GPa	13.8GPa	82GPa
Poisson's ratio	0.36		0.43	
Coefficient of thermal expansion	$70x10^{-6}/^oC$		$10x10^{-6}/^oC$	

The specimen's design was depicted on Figure 1, and the stress-strain curves derived from the TiNi fiber at different temperature were on Figure 2. The diameter of the shape memorized TiNi fiber (Ti=50%, Ni=50%) was 0.4 mm. It was molded and kept 30minuts in 500 ^oC for curing. Then they were quenched in iced water. Four transformation temperature of the TiNi fiber was determined; martensitic start M_s=31 ^oC, martensite finish M_f=15 ^oC, austenitic start A_s=57 ^oC, and austenitic finish A_f=63 ^oC. Prior to heat treatment the shape-memorized TiNi fiber was given

three different tensile prestrain; ε=0, 1, 3%. While heat treating polycarbonate, temperature might exceed A_f of the TiNi fiber. The process might cause the embedded TiNi fiber to be shrunk. Avoiding shrinkage during the process, TiNi fiber was fixed by the jigs to keep its prestrain. The volume fraction (V_f) of TiNi fiber in the specimen is 0.8%. 0.9 mm deep side notch (V-shape) with a notch-tip angle 30^o was then cut into the molded composite specimens by the microtome. Prior to the experiments, a 100 μm (1 grid) length pre-fatigue crack was generated on the specimen by applying cyclic, constant stress, σ_{max}=4.6MPa. Using 60μm diameter dots, 100 μm orthogonal fine dotted grids were deposited on the surface of the polycarbonate specimens by a vacuum evaporator for local strain measurement near a crack-tip. The fine dotted grids were shown on Figure 1.

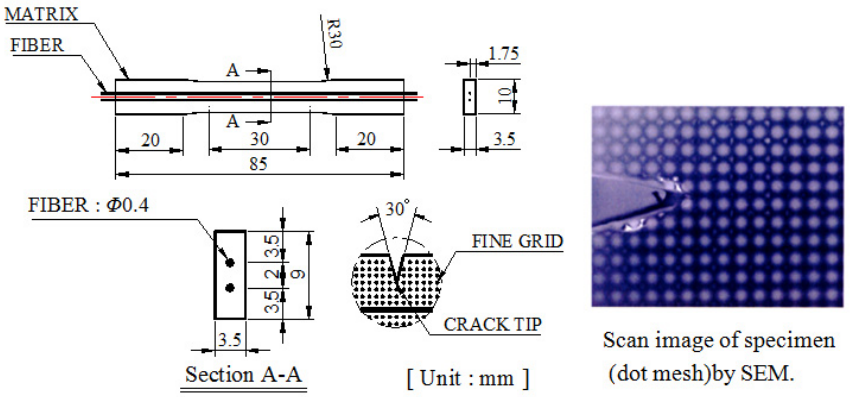

Figure 1: Geometry of TiNi / Polycarbonate composite specimen

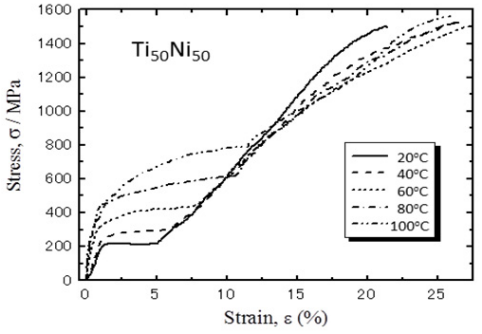

Figure 2: Stress-strain curves of TiNi fiber at different temperatures

2.2 Fatigue test

The devices used in the experiments were; a scanning electron microscope (JSM-5410LV, JEOL), and fatigue testing machine (SEM servopulser, SHIMADZU, with capacity 5kN, +-25mm).

Figure 3 showed the experimental devices. The fatigue crack propagation tests were performed by the K-increasing method.

Figure 3: Experimental apparatus

In the method, ΔK increased during crack propagation progression under a constant cyclic stress range ($\Delta\sigma$). The applied stress was triangular wave with stress ratio, $R=\sigma_{min}/\sigma_{max}=0$, and $\sigma_{max}=4.6$MPa. Its repetition frequency was 0.6Hz in the near vacuum state. When a fatigue crack reached 4 grids (400 μm) at 20 ^{o}C, the ambient temperature in the SEM servopulser was raised to 80 ^{o}C. Then, stress was applied again until complete failure of the specimen.

Deformed fine grids at the crack-tip were recorded each cycle for the every specimen. Based on these observations, crack length and grids length were calculated.

The amount of the crack opening displacement ($\Delta CTOD$) was calculated starting from non-stressed three grids length (300 μm). Measurement unit was one grid length (100 μm). Fatigue crack propagation rate (da/dN) was calculated from the slope of the line which describes the relationship between crack lengths and cyclic numbers. Stress intensity factor range (ΔK) was obtained by using the following formula;

$$\Delta K = Y\Delta\sigma\sqrt{a} \tag{1}$$

where Y denoted the finite width compensation coefficient, and a was the crack

length. Here, a was for a crack in the polycarbonate matrix and did not include the crack in the domain near the embedded TiNi fiber. For the specimens with the side-crack, Y was determined using follow formula.

$$Y = 1.99 - 0.41(a/w) + 18.70(a/w)^2 - 38.48(a/w)^3 + 53.85(a/w)^4 \quad (2)$$

3 Results and discussion

3.1 Control of fatigue crack propagation by shape memory effect

Figure 4 showed examples of the relationship between crack length a and cyclic loading number N for the specimens. The given tensile prestrain was 0, 1, or 3% and applied stress, which was parallel to the notch of specimen, had σ_{max}=4.6MPa and σ_{min}=0MPa.

In any cases a crack propagated slowly when it started. It rapidly propagated when cycle reached 26.6×10^3(for 0%), 62.8×10^3(for 1%) and 139.2×10^3(for 3%) cycles.

Temperature in the SEM servopulser was, then, raised to 80 ^{o}C ($> A_f$) from 20 ^{o}C. As the ambient temperature was raised, crack propagation with 1and 3% tensile prestrain slowed down and almost stopped compared to one with 0% prestrain.

To observe further cyclic loading number was increased 15% (118×10^3cycles) for 1% prestrain and 20% (187.9×10^3cycles) for 3% prestrain.

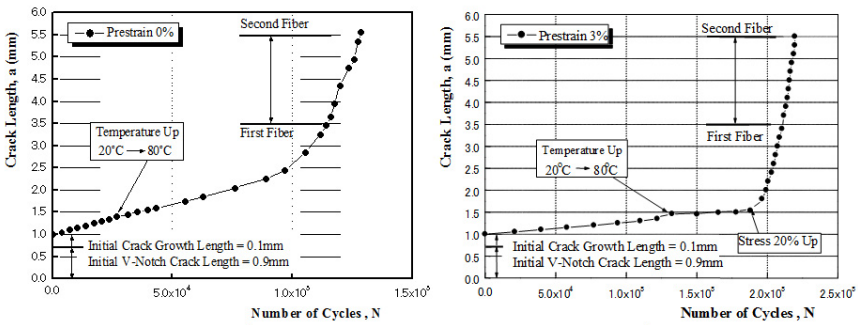

(a) Prestrain 0% (b) Prestrain 3%

Figure 4: Experimental crack length versus number of cycles.

Figure 5 showed the scan images on 3% prestrain specimen by the SEM and Figure 6 depicted the relationships between fatigue crack propagation rate (da/dN) and stress intensity factor range (ΔK) for 1 and 3% prestrain.

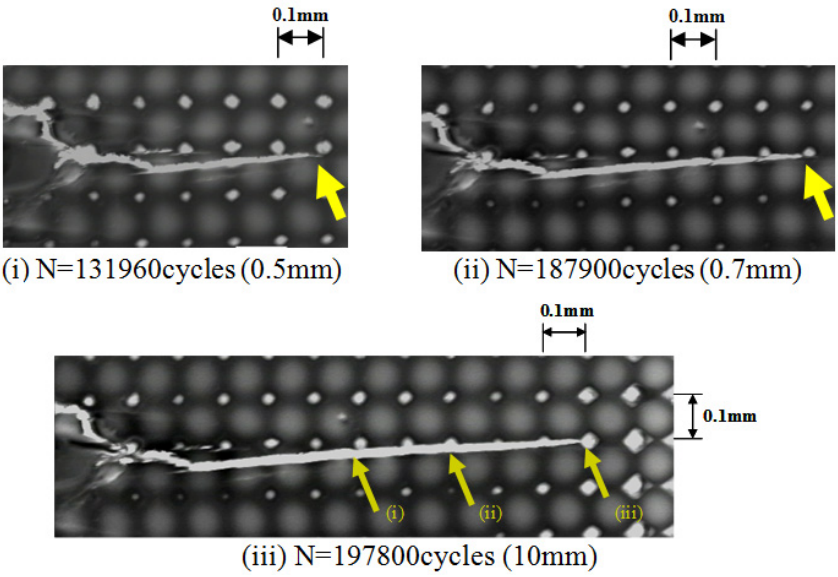

Figure 5: Scan images of fatigue crack growth at prestrain 3% by SEM.

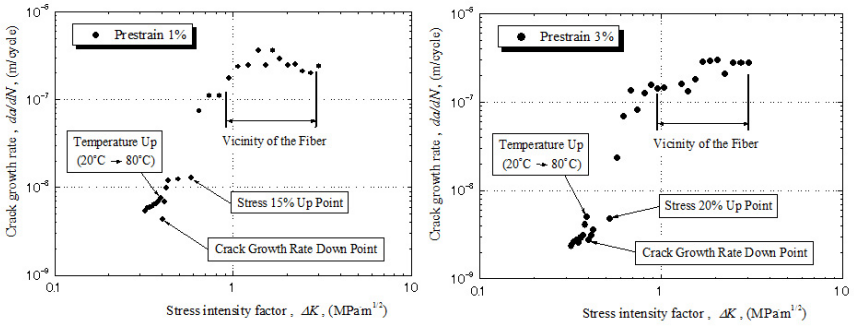

(a) Prestrain 1% (b) Prestrain 3%

Figure 6: Fatigue crack growth versus stress intensity factor for TiNi/PC composite.

It clarified the suppression effect to fatigue crack propagation, and also showed the interesting fact that more prestrain lead greater suppression effect. With 1% prestrain, fatigue crack propagation rate was 57% less than that of 0% when raising the temperature to 80 ^{o}C from 20 ^{o}C. With 3% prestrain, fatigue crack propagation rate was 73% less than that of 0%.

In addition, the crack propagation rate in the domain near the TiNi fiber was rapidly reduced although cyclic loading numbers were increased further. The continuous

fatigue crack closure mechanism would be presented because of the shape memory (shrinkage) effect of the TiNi fiber, and energy release by Martensite transformation (superelasticity) in the vicinity of a crack tip when temperature in SEM servopulser was at or above A_f.

3.2 Local fatigue crack-tip deformation behavior

The large residual compressive stress associated with the shape memory shrinkage of the embedded TiNi fiber mentioned above reduced the stress concentration at the crack tip. Moreover, it also changed a fatigue crack closure phenomena. Figure 6 showed a fatigue crack propagation path when the crack propagation rate was changed.

By using real-time fine grid strain measuring technique (Shimamoto, Yokota, Furuya & Takahashi 1988) the hysteresis loops, the relationship between applied external stress (a) and crack-tip opening displacement U (*CTOD*), were investigated. The U (*CTOD*) values were measured at the point (X=-200 μm) behind a propagating crack-tip.

Figure 7 showed the variations of the σ-U (*CTOD*) hysteresis loops for two different prestrain values, ε=1% and ε=3% in different temperature in the SEM servopulser; temperature=20^{o}C and after temperature=80^{o}C, heating above A_f temperature, respectively.

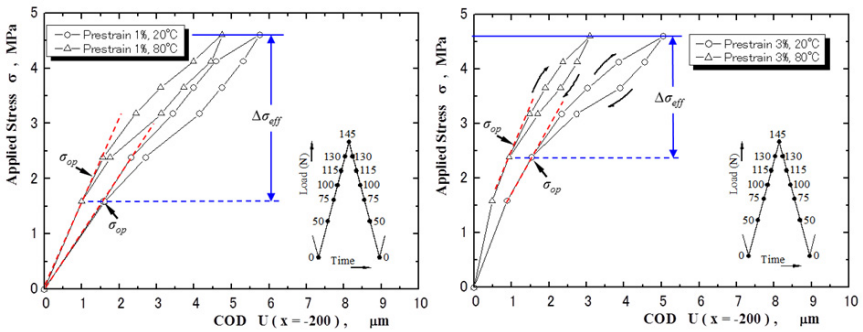

(a) Prestrain 1% (b) Prestrain 3%

Figure 7: Applied stress versus crack opening displacement (*COD*) before and after heating above austenite finishing temperature (A_f).

CTOD decreased rapidly and crack-opening stress (σ_{op}), which was defined at the crooked point (i.e. arrow point) in the middle of a loading cycle, increased after temperature was raised. Δ*CTOD* decreased 11% for ε=0%, 17.4% for ε=1%, and

38.8% for ε=3% right after raising the temperature in the SEM servopulser. The crack propagation rate for ε=1% was reduced 1.4 times as much as that of ε=0%. Similarly, the crack propagation rate for ε=3% was reduced 2.8 times as much as that of ε=0%. The effective cyclic stress range ($\Delta\sigma_{eff}$ =$\Delta\sigma_{max}\Delta\sigma_{ep}$) for ε=3% decreased as much as 50% more than ε=1% with temperature above A_f (80 ^{o}C).

3.3 Comparison between theoretical analysis and experimental

3.3.1 Fatigue crack propagation retardation

As shown in σ-U hysteresis loops for ε=3% in Figure 7 (b), stress increase σ_{up}= σ_{op}(80 ^{o}C) - σ_{op}(20 ^oC)=1.5MPa corresponded to σ_m, the residual compressive stress in the matrix due to the TiNi fiber compressive effect. Eshelby's equivalent inclusion model predicted that the compressive stress value, σ_m, in the matrix became the value near -6.3MPa (Taya, Furuya 1993). The difference between theory and experiment would arise mainly from the incomplete bonding at the interface of fiber and matrix. The difference, however, did not deteriorate the fact that the large compressive residual stress could be actively introduced by the shape memory shrinkage of the TiNi fiber in the composite. It effectively reduced the stress intensity at a crack-tip, and suppresses fatigue crack propagation.

3.3.2 Crack propagation behavior within a domain very near the embedded TiNi fiber

Figure 8 and Figure 9 showed changes in the K value in the neighborhood of the embedded TiNi fiber. Figure 8 was the K value variations from the theoretical analysis by the elastic fracture mechanics theory (Fujino, Sekine, Abe 1984). Figure 9 was the changes in the K value when crack length a and a finite width w increased; where G was the stiffness of a semi-infinite composite, a was the crack length, I was the distance from surface of a specimen to fiber, $G*$ was the stiffness of fiber, and ν is the Poisson ratio.

Figure 8 suggested if there was steady stress σ_o in the matrix, greater stress σ_o* was also created in the embedded TiNi fiber. The changes in the K value, which corresponded to crack length a, depended on a non-dimensional parameter (Γ) that was related to the volume function ratio (h/l) as well as the stiffness ratio ($G*/G$). Figure 11, however, indicated that the K value was apt to decrease exponentially as it approached to the TiNi fiber. With a finite width (W_o) specimen, the actual K value was inevitably affected by another increasing factor; finite width correction factor $Y(a/W_o)$. The actual K value in the specimens might not be changed so much because of the cancellation of the two factors; inhomogenity (-) and finite correlation (+) as shown in Figure 9 curve (A) and (B). Figure 9 curve (C) suggested

that the effect of the decreasing K value was weakened in the neighborhood of the TiNi fiber.

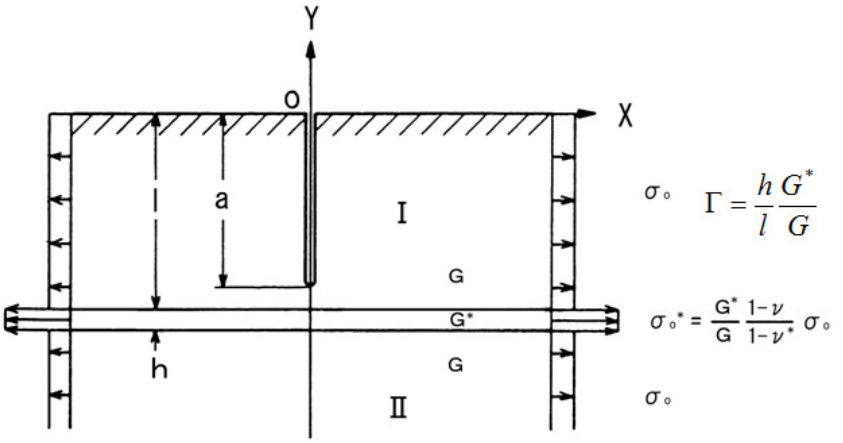

Figure 8: An edge crack in a semi-infinite composite with a long reinforced phase and a coordinate system.

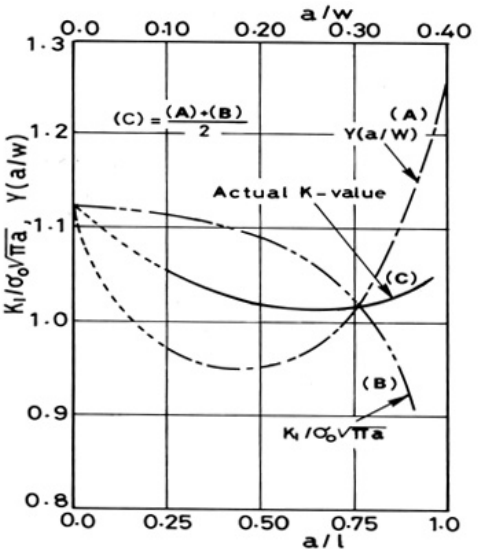

Figure 9: Estimation of the variation of actual of K_I value with increasing the crack length (a) of the test specimen with finite width (W)

The behavior of the *CTOD* when approaching the TiNi fiber was also investigated to verify domain effect. It gradually decreased as a crack-tip approached to the domain near the embedded TiNi fiber and finally it was saturated at a constant small value when a fatigue crack began to arrest at the domain region D. This typical fatigue crack arresting phenomena was related to the theoretically predicted decrease of the K value at the domain area very near reinforced fiber.

4 Conclusions

Fatigue crack propagation behaviors and local strain at a crack tip in the SMA polycarbonate composite were investigated by utilizing the fine-grid method, which allowed the measurement of the crack tip opening displacement through the distortion of grid at a crack-tip in one loading cycle. From the presented results, following conclusions were drawn:

Fatigue crack propagation was arrested or retarded immediately after heating the specimens at and above A_f temperature, and the effect depended on the pre-strain of embedded TiNi fiber.

The compressive stress in the polycarbonate matrix also contributed to reduce stress intensity at a crack tip and decrease fatigue crack propagation rate.

The continuous fatigue crack closure mechanism would be presented because of the shape memory (shrinkage) effect of the TiNi fiber, and energy release by Martensite transformation (superelasticity) in the vicinity of a crack tip when temperature in SEM servopulser was at or above A_f

References

Rogers CA.; Liang C.; Lee S. (1991): Proceedings of the 32nd Structures, Structural Dynamics and Materials Conference (AIAA, Washington, Part), pp.1190.

Chaudhry Z.; Rogers CA. (1991): J Intelligent Mater Syst Struct, vol.2. pp.581.

Furuya Y.; Sasaki A., (1993): Taya M. Enhanced mechanical properties of TiNi shape memory fiber /AI matrix composite.: Mater. Trans. JIM34, pp.224-227.

Shimamoto A.; Umezaki E. (1995): Fatigue crack-tip deformation crack growth and life prediction in limited part crack tip in spread process Exp. Mech., vol.35, no.3, pp. 251-256.

Shimamoto A.; Taya M (1993): Crack close action of composite material which uses shrinkage effect of shape memory TiNi embedded fiber. JSME 63-605A., pp.26-31.

Shimamoto A.; Furuya Y.; Taya M (1997): Fatigue crack spread control by shape memory TiNi fiber reinforced composite. JSME, Lecture of the 74th stage thesis

collection (1), pp.667-668.

Shimamoto A.; Furuya Y.; Taya M (1999): Crack close action of composite material which uses shrinkage effect of shape memory TiNi embedded fiber(effect of domain size). JSME65-634A, pp.1282-1286.

Shimamoto, A.; Hawong JS.; Lee HJ (2002): Development of Shape Memory TiNi Fiber Reinforced Epoxy Matrix Composite and Its Properties Transactions of the ASME, vol.124, pp.390-396

Shimamoto A.; Azakami T.; Oguchi T (2003): Reduction of K_I and K_{II} by the Shape-memory Effect in a TiNi Shape-memory Fiber-reinforced Epoxy Matrix Composite Exp. Mech., vol 43, no.1, pp.77-82.

Shimamoto, A.; Zhao, H.Y.; Abe, H. (2004): Fatigue crack propagation and local crack-tip strain behavior in TiNi shape memory fiber reinforced composite International Journal of Fatigue 26, pp.533-542.

Shimamoto A.; Takahashi S.; Yokota A. (1991): Fundamental study on rupture by low-cycle fatigue of polymers applying the five-grid method. Exp. Mech., vol.31, no.1, pp. 65-69.

Shimamoto A.; Umezaki E.; Nogata F.; Takahashi S (1992): Strain behavior near fatigue crack tip in polycarbonate and its life evaluation. JSME 58-555A, pp.2023-2027.

Shimamoto A.; Umezaki E (1995): Fatigue crack-tip deformation crack growth and life prediction in polycarbonate. Exp Mech, vol.35, no.3, pp.251-256.

Shimamoto A (1999): Fatigue crack initiation of polycarbonate material and strain behavior in limited part crack tip in spread process.JSME65-635A, pp.1534-1538.

Taya M.; Furuya Y.; Yamada Y.; Watanabe R.; Shibata S.; Mori T. (1993): Strengthening mechanism of TiNi shape memory fiber/AI matrix composite. In: Varadan VK, Ceditor. Proceedings of Smart Mater, vol.1916 SPIE, pp.373-383.

Fujino K.; Sekine H.; Abe H. (1984):Analysis of an edge crack in a semi-infinite composite with a long reinforced phase. Int. J. Fract 25, pp.81-94.